

Sublinear temperature dependence of thermal conductivity in the incommensurate phase of TlInTe₂

Naini Bajaj ¹, Dhanashree Chemate,² Harish P. Veeravenkata,¹ Ashish Khandelwal ³, M. K. Chattopadhyay,^{3,4} Moinak Dutta,⁵ Aditya Prasad Roy ¹, Archana Sagdeo,⁶ Ankit Jain,¹ Shriganesh S. Prabhu ², Kanishka Biswas,⁵ and Dipanshu Bansal ^{1,7,*}

¹Department of Mechanical Engineering, Indian Institute of Technology Bombay, Mumbai, Maharashtra 400076, India

²Department of Condensed Matter Physics & Materials Science, Tata Institute of Fundamental Research, Mumbai, Maharashtra 400005, India

³Free Electron Laser Utilization Laboratory, Raja Ramanna Centre for Advanced Technology, Indore, Madhya Pradesh 452013, India

⁴Homi Bhabha National Institute, Training School Complex, Anushakti Nagar, Mumbai, Maharashtra 400094, India

⁵New Chemistry Unit, Jawaharlal Nehru Centre for Advanced Scientific Research, Jakkur, Bangalore 560064, India

⁶Synchrotron Utilization Laboratory, Raja Ramanna Centre for Advanced Technology, Indore, Madhya Pradesh 452013, India

⁷Center for Research in Nano Technology and Science, Indian Institute of Technology Bombay, Mumbai, Maharashtra 400076, India



(Received 14 January 2022; revised 29 September 2022; accepted 18 November 2022; published 2 December 2022)

Thermal conductivity (κ) of semiconducting and insulating solids generally show inverse linear temperature dependence above the Debye temperature (T_D) owing to dominant phonon-phonon scattering, i.e., $\kappa \propto T^{-1}$. Recently, in ultralow κ materials, κ is found to decrease sublinearly ($\kappa \propto T^{-\alpha}$ where $0 < \alpha < 1$) above T_D as interbranch wavelike tunneling contribution becomes significant. Here we show that the deviation from linearity can be unprecedentedly large in incommensurate (IC) phases as exemplified by archetypal Zintl-like semiconductor TlInTe₂. This happens because two mutually incompatible translational symmetries allow spatially and temporally varying phase shifts, thus giving rise to two new heat-carrying modes: phasons and amplitudons. Using comprehensive transport and spectroscopy measurements combined with first-principles simulations of multichannel thermal transport, i.e., phonon-phonon scattering and tunneling contributions, we find that new modes contribute nearly 10-30% of the total κ near the IC transition. The origin of this IC transition is rooted in the TI lone pair and large polarizability of the electronic cloud, whose fingerprints are visible in the phonon linewidths. Our study paves the way for understanding ultralow κ in IC phases, particularly for charge-density-wave materials where IC modulation is ubiquitous.

DOI: [10.1103/PhysRevB.106.214101](https://doi.org/10.1103/PhysRevB.106.214101)

I. INTRODUCTION

In Peierls Boltzmann transport equation of nonmagnetic semiconducting and insulating solids above the Debye temperature T_D , thermal conductivity (κ) is inversely proportional to temperature, i.e., $\kappa \propto T^{-\alpha}$, where α is equal to one [1–3]. The α can be greater than one for (molecular) solids having a dynamic disorder or strong quasiparticle coupling (super-linear T dependence) before κ plateaus at high temperatures and approaches the minimum value κ_{\min} . [1] Recent measurements have shown that ultralow thermal conductivity materials, such as CsPbBr₃ and Tl₃VSe₄, have $\alpha < 1$, [4,5] which is now understood to originate from a combination of Peierls contribution and coherences term. [6] The Peierls contribution stems from phonon-phonon scattering processes, i.e., Umklapp processes, while the coherence term is due to interbranch wavelike tunneling enabled by overlapping phonon branches and finite phonon linewidths. [4,6] On heating, the Peierls contribution κ_P decreases as $\kappa_P \propto T^{-1}$ (assuming minimal renormalization of interatomic forces). In contrast, the coherences term κ_C increases with temperature due to increased interbranch wavelike tunneling, thus enabling $\alpha < 1$

temperature dependence. [6] Besides the above mechanisms, phonon renormalization in strongly anharmonic materials or near phase transitions leads to nontrivial changes in phonon group velocity (v_g) and phonon-phonon (ph-ph) scattering phase space. The renormalized phonons may lead to deviation from $\alpha = 1$ in a limited T range near the transition as recently observed for SnS and SnSe, [7] or at high T as reported for PbTe. [8,9]

Incommensurate (IC) phases offer an extra degree of freedom for thermal transport due to two or more different translational symmetries with continuously accumulating phase shifts ϕ between them. [10–12] If we consider ϕ' to be derivative of the phase with respect to the site coordinates along which the phase is being accumulated, we get two new dynamical modes, namely phasons and amplitudons, corresponding to purely tangential sliding and radial breathing in ϕ' , respectively {see pictorial illustration in Supplementary Materials (SM) Fig. S1, [13] see also Refs.[14–30] therein}. The energy-wavevector relationship, i.e., dispersion, of phasons and amplitudons, is similar to acoustic and optic modes, as shown in Fig. 1(d). However, as the IC lattice is significantly larger, the Brillouin zone is proportionally reduced (see SM Fig. S2); consequently, the contribution of phasons and amplitudons towards heat capacity (C_p) is small. [31,32] But phason group velocity (v_g) is not limited by the speed

*dipanshu@iitb.ac.in

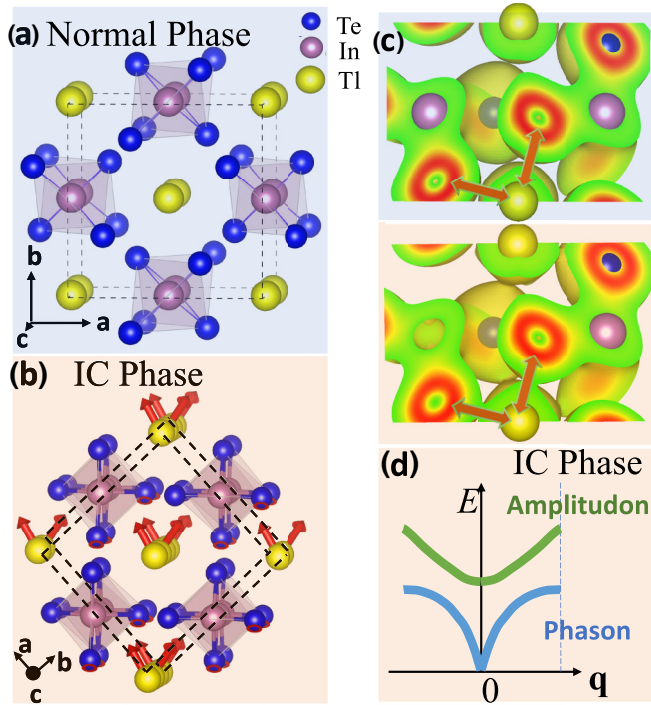


FIG. 1. (a) Crystal structure of TIInTe₂ in the normal phase as viewed along the *c* axis. The In atom is covalently bonded (sp^3) to four Te atoms forming InTe₄ tetrahedrons and the chains of Tl cations reside in between the tetrahedrons. (b) Tl atoms move towards the InTe₄ tetrahedrons and towards each other (shown by red arrows) leading to incommensuration along the *c* axis. (c) Distribution of charge density in the normal phase (top panel) and the IC phase (bottom panel). IC modulation leads to overlap of the Tl-In charge cloud (indicated by the orange arrows) and bond formation. (d) Qualitative dispersion curves of amplitudon and phason excitations in the IC phase arising from two or more different translational symmetries with continuously accumulating phase shifts (see SM Fig. S1). These excitations resemble optic and acoustic modes of a crystal.

of sound and can travel subsonically and supersonically; for example, supersonic velocities are observed in blue bronze [33] and fresonite crystals, [12] hence contribution to κ is not necessarily negligible ($\kappa = \frac{1}{3}C_p v_g^2 \tau$, see SM Fig. S2). Here τ is the phonon/phason lifetime.

So far, phason thermal transport is studied in metals where charge-density-wave (CDW) instability leads to the IC lattice rearrangement below T_{CDW} , for example: (TaSe₄)₂I, (NbSe₄)₁₀I₃, K_{0.3}MoO₃, TaS₃, and (Na,K)_{0.9}Mo₆O₁₇, [34,35] but challenges remain in deciphering the phason contribution to κ . In the IC CDW phase, electronic states are partially or fully gapped at the Fermi level (E_F) with bound electron-hole pairs. Hence both polar (i.e., Wiedemann-Franz) and bipolar terms contribute to κ . [34] Moreover, the gapped state at E_F decreases the electron-phonon (e-ph) scattering phase space as energy and momentum conservation of the e-ph system can not be satisfied, thus increasing both phonon and electron lifetimes. [36,37] Hence, the estimation of all these contributions in both metallic and IC CDW phase to isolate the phonon and phason contributions is generally not straightforward. The IC phase in semiconducting and insulating materials, in particular where the IC phase exists near T_D , is ideally

suitable for thermal transport study, as electronic contribution and e-ph scattering are both absent. Previous studies in known insulating IC phases such as Hg_{3- δ} AsF₆, Rb₂ZnCl₄, β -ThBr₄, C₁₂D₁₀, K₂SeO₄, and NaNO₂, focused commensurate to IC transition and did not investigate the thermal transport. [10,38–49] Moreover, the IC transition temperature was away from T_D , thus was not ideal for unambiguously establishing deviation from $\kappa \propto T^{-1}$ in the IC phase.

Zintl-like electron-deficient semiconductors TIMX₂ ($M = \text{Ga, In}$; $X = \text{S, Se, Te}$; $E_g \sim 1 \text{ eV}$) stabilize in the IC phase in a wide temperature range near T_D , [50] and have recently garnered interest for ultralow $\kappa \sim 0.5 \text{ Wm}^{-1}\text{K}^{-1}$ at 300 K. [14,28–30,51] These semiconductors are promising candidates to probe inverse T dependence and isolate the phason contribution to κ . With this study, we elucidate on the sub-linear thermal transport ($0 < \alpha < 1$) of TIInTe₂ in normal, IC, and commensurate phases using both frequency and time-domain spectroscopy and detailed first-principles simulations by explicitly calculating κ_P and κ_C with and without (w/o) phonon renormalization. Our direct measurements of the imaginary part of the dielectric constant allow us to exclude the presence of charge carriers near the Fermi level and their interaction with phonons. We find phasons and amplitudons contribute nearly 10 to 30% to the total κ near the IC phase transition. The phason and amplitudon contribution combined with renormalized κ_P and κ_C enable sublinear T dependence ($0.7 \leq \alpha \leq 0.8$) in a wide temperature range spanning 100 to 400 K. The origin of the IC phase is rooted in the large polarizability of Tl lone pairs, and we trace its fingerprints in the linewidths/lifetimes of multiple phonon modes.

II. NORMAL-INCOMMENSURATE-COMMENSURATE PHASE TRANSITIONS

TIInTe₂ crystallizes in the tetragonal body-centered lattice with $D_h^{18} - I4/mcm$ space group at room temperature (RT), [14,50] as confirmed by our x-ray diffraction measurements (see SM Fig. S3). Figure 1(a) shows the crystal structure of TIInTe₂ in the $a - b$ plane consisting of alternating (InTe₄)¹⁻ anionic and Tl¹⁺ cationic chains along the *c* axis. Within the (InTe₄)¹⁻ tetrahedrons, In is covalently bonded (sp^3) to four Te atoms. Each tetrahedron shares its horizontal edges to adjacent tetrahedra along the *c* axis. Since sp^3 hybridized In has three valence electrons, it cannot form two-center-two-electron bonds with Te atoms. Thus, analogous to 1D Zintl compounds, TIInTe₂ is electron deficient and adopts a Zintl-like structure. [14] Tl atoms reside in between the anionic chains surrounded by eight Te atoms. They donate an extra electron to the anionic chain to attain formal valence of +1. Tl-Te distance of 3.59 Å is significantly larger than the sum of the covalent radii of Tl (1.45 Å) and Te (1.35 Å), but is close to the sum of the ionic radii; consequently, the mean square displacements (MSD) of Tl are nearly a factor of two larger than In and Te at RT. [30] The large MSD has implications on the measured phonon spectra, as we discuss later.

Similar to TIInSe₂, [50,52] in the IC phase of TIInTe₂, Tl atoms move towards the InTe₄ tetrahedrons and towards each other leading to incommensuration along the *c* axis [see Fig. 1(b)]. This movement leads to the increased overlap of Tl-Te charge cloud, as illustrated in Fig. 1(c) top and bottom

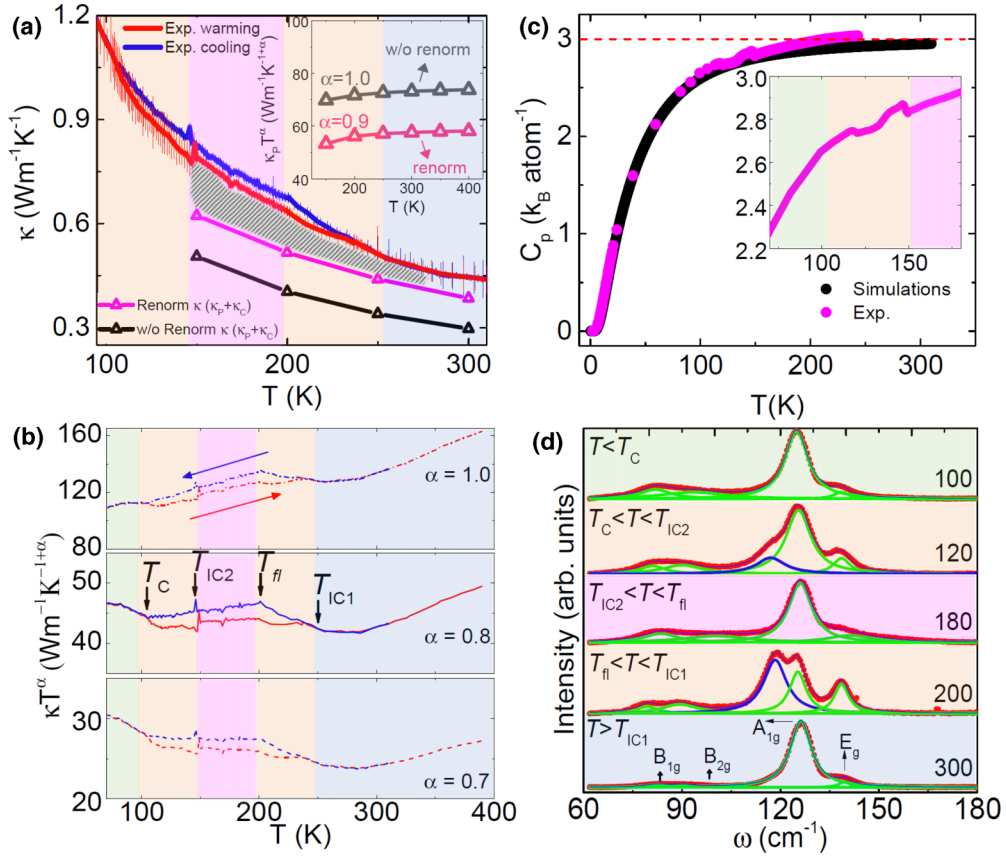


FIG. 2. (a) κ of TIInTe₂ between 100–300 K measured on heating (red) and cooling (blue) cycle (Run 1) compared with simulated $\kappa = \kappa_p + \kappa_c$. Renorm refers to simulated κ accounting for temperature-induced renormalization of interatomic force constants, while w/o renorm is without renormalization. The shaded area indicates the contribution of phasons and amplitudons to κ . Inset: Simulated $\kappa_p T^\alpha$ approaching constant value above T_D for $\alpha = 0.9$ and 1.0 for renorm and w/o renorm, respectively. (b) Variation of κT^α on heating and cooling for $\alpha = 0.7, 0.8$, and 1.0 . T_{IC1} , T_{fl} , T_{IC2} , and T_C indicate the first IC transition, fluctuation regime transition, second IC transition, and commensurate transition temperatures. (c) C_p measurements from 2 to 240 K compared with simulations. The red dotted line indicates constant volume high- T limit of 3 k_B/atom. Inset: enlarged view of C_p in the 75–175 K range showing the transition near 150 K. (d) Raman active modes in different phases on cooling. At 200 and 120 K, the blue peak near 115 cm⁻¹ is the amplitudon mode that appears in the IC phase but is absent in the normal and commensurate phases.

panels, showing two-dimensional cuts of charge-density distribution with and w/o the IC modulation. We confirm this observation by directly tracking specific TI-Te and In-Te distortions using spectroscopy measurements, as discussed later. Below we identify the series of normal-IC-commensurate phase transitions as evident from anomalies/kinks in the κ , C_p , and diffraction measurements.

Figure 2(a) shows measured κ on heating and cooling between 90 and 310 K. A thermal hysteresis is visible between 100 and 240 K, which is repeatable in different runs (see SM Fig. S4). The present experimental values of κ are consistent with previous measurements performed above RT. [14,29] A series of transitions are evident from data, which we denote in Fig. 2(b). At RT, TIInTe₂ is stable in the normal phase. On cooling below $T_{IC1} \sim 233$ K, TIInTe₂ transitions to the IC phase as indicated by the change of slope of $\kappa(T)$ and the appearance of amplitudon mode in the Raman scattering measurements [see the blue peak in Fig. 2(d)]. A kink at T_{IC1} is also visible in the intensity of (2,2,2) and (2,0,0) Bragg peaks (see SM Fig. S5). We have color-coded the figure background for easy visualization of different phases. However, the IC

phase below T_{IC1} is not stable due to thermal fluctuations. Below $T_{fl} \sim 200$ K, we observe that the amplitudon mode disappears, and a kink appears in κ and Bragg peaks intensities, as TIInTe₂ transitions back to the normal phase. On further cooling, the IC phase is locked in below $T_{IC2} \sim 146$ K, as evident from the reappearance of the amplitudon mode, and sharp anomalies in κ and C_p [see Fig. 2(c)]. Near $T_C \sim 117$ K, a shallow peak is visible in $C_p(T)$, which, we believe, indicates the transition to the commensurate phase. This is consistent with the disappearance of the amplitudon mode below 120 K as shown in Fig. 2(d). While the signature of T_C is not obvious in κ , the closure of the hysteresis loop below 106 K and sharp kink in Bragg peaks intensities indicate that this first-order phase transition is complete. The hysteresis in the IC phase is understood to originate from defects/disorders that obstruct diffusion of discommensurations, thus preventing crystal to thermally equilibrate, as demonstrated for IC phase transition in Rb₂ZnCl₄. [40] Here we note, while the IC and commensurate phases are well established in literature for TI GaTe₂ and TI In(S,Se)₂, [17,50,53–57] previous measurements and simulations of electrical conductivity

[14,58–60] and κ , [14,28,29,51,60] C_p , [14] Hall effect [58], x-ray diffraction, [17,30] and thermal expansion [61] on TlInTe₂ did not yet identify different phases; however, compressibility data did show anomaly at T_{IC1} and T_C . [61] The lack of observation in previous measurements may be related to the disorder-induced broadening of the first-order transition. [62] Disorders obstruct the motion [62] of the IC phase boundaries during the nucleation and growth of phases and smear out these first-order transitions and widen the regime of metastability. However, if the temperature change is not strictly unidirectional, thermal fluctuations destroy the metastability. Such first-order transitions may be difficult to detect, especially in the absence of any sudden discontinuity in the measured κ as explained in the next section.

III. TEMPERATURE DEPENDENCE OF κ

Figure 2(b) shows κT^α as a function of T for $\alpha = 1.0, 0.8$, and 0.7 . The T_D of TlInTe₂ calculated from mean phonon energy is 144 K and is consistent with literature data. [51,61] As discussed earlier, if phonon renormalization is minimal, we should obtain a constant value of κT^α for $T > T_D$ for $\alpha = 1.0$. However, as we observe, κT^α approaches a constant value for $0.7 \leq \alpha \leq 0.8$, instead for $\alpha = 1.0$. This α value suggests possible role of other degrees of freedom to κ .

In Fig. 2(a), we compare measured κ with simulated $\kappa_P + \kappa_C$ with and w/o T -induced phonon renormalization. As we can see, simulated values are lower than measured κ in the entire T range above T_{IC2} [below T_{IC2} , the IC unit cell is too large (> 1000 atoms) for available computational resources]. Here, we emphasize that accurate phonon calculations necessitated $6 \times 6 \times 6$ q -grid in density functional perturbation theory (DFPT) simulations, which are in excellent agreement with measured phonon density of states (DOS) (see SM Fig. S6 and S7). Reproducing experimental phonon peaks is essential for three-phonon scattering phase space calculations, and subsequently, for obtaining converged values of κ_P and κ_C (see SM for details and SM Fig. S8). Inset of Fig. 2(a) shows $\kappa_P T^\alpha$ with and w/o renormalization. As expected, $\kappa_P T^\alpha$ w/o renormalization approaches constant value for $\alpha = 1.0$. On the other hand, renormalized $\kappa_P T^\alpha$ becomes flat for $\alpha = 0.9$, thus indicating a change in three-phonon scattering phase space with increasing T owing to the phonon renormalization. With and w/o renormalization, κ_C has a small contribution ($< 15\%$) below 300 K but becomes comparable to κ_P above it (see SM Fig. S9).

Hence, it is apparent that simulated $\kappa_P + \kappa_C$ cannot alone account for the measured sublinear α between 0.7–0.8. The other possibilities of sublinearity could include electron/free carrier contribution to κ , electron-phonon or free carrier-phonon scattering, lattice impurities, or grain boundaries. [1–3] We rule out any contribution from electrons or free carries in the next section. Moreover, our XRD measurements did not show any trace of impurities within experimental uncertainty (see SM Fig. S3) and the minimum grain size, as estimated from scanning electron microscopy, is ~ 1 -2 μm ; hence it does not affect the reported κ . We highlight the difference between simulated and measured κ using the shaded area in Fig. 2(a). Hence, in the absence of electronic/free carrier, impurity, and grain boundary contributions, this

difference must originate from κ_{IC} (i.e., phasons and amplitudons contribution to κ), which is nearly 20% of total κ at T_{IC2} . We emphasize that despite the careful comparison with measured phonons and converge studies of κ_P and κ_C , the simulated total κ will have uncertainty; similarly error bars on measured κ can be as large as 10% [see Fig. 2(a)]. The uncertainty in simulations and error bars in experiments may slightly decrease or increase estimated κ_{IC} from 20%, but the reported sublinearity owing to κ_{IC} is robust. Moreover, it is not surprising that κ_{IC} , albeit small, extends above T_{IC1} . This is due to thermal fluctuations that enable phason intensity to appear more than 100 K above the IC transition, as experimentally observed for feresonite crystals. [12] Moreover, below T_{IC2} , as IC wavevector continuously moves towards commensuration, the accumulated phase shifts will decrease; hence κ_{IC} will slowly decrease to zero as we approach T_C . This continuous evolution of κ_{IC} , within and above the IC phase, prevents any sudden discontinuity in measured κ . Furthermore, C_p is well-reproduced in simulations in the entire T -range [Fig. 2(c)], as it primarily depends on phonon DOS. As described earlier and illustrated in SM Fig. S2, phasons have relatively small DOS; hence their contribution to C_p is generally small.

IV. ELECTRONIC CONTRIBUTION TO THERMAL TRANSPORT

TlInTe₂ is an indirect bandgap (~ 0.73 eV) [63] semiconductor. At RT, the electronic contribution is expected to be negligible. Indeed, from the measured electrical resistivity [SM Fig. S10(a)], the electronic contribution to κ is found to be several orders of magnitude smaller than phonons; hence we can safely exclude it. The carrier concentration calculated from Hall measurements also has a relatively low value of $\sim 1.3 \times 10^{17}$ cm^{-3} at room temperature (see SM). However, despite a low concentration, if the carriers are present near the Fermi level (E_F), they can scatter phonons [37] and reduce κ by 10 to 30%, as experimentally demonstrated for photoexcited silicon. [64] We measured the real and imaginary parts of refractive index ($RI = n + ik$) and dielectric constant ($\epsilon = \epsilon' + i\epsilon''$) using THz time-domain spectroscopy [see Fig. 3(b) and SM Fig. S11]. If carriers were present near E_F , we would get diverging n , k , ϵ' , and ϵ'' at zero frequency ($\omega \rightarrow 0$), as qualitatively illustrated in Fig. 3(a). [65] However, the measured data down to 0.25 THz do not show diverging behavior. Thus, we can conclude that carriers play a minimal role in thermal transport. Below we focus on anharmonic lattice vibrations leading to ultralow κ in TlInTe₂.

V. ANHARMONIC TL VIBRATIONS WITHIN RIGID InTe₄ SUBLATTICE

As we described earlier, Tl atoms undergo larger thermal displacements than In and Te ($U_{11}^{\text{Tl}} = U_{22}^{\text{Tl}} = 0.035$ \AA^2 , $U_{33}^{\text{Tl}} = 0.038$ \AA^2 , $U_{11}^{\text{In}} = U_{22}^{\text{In}} = 0.021$ \AA^2 , $U_{33}^{\text{In}} = 0.015$ \AA^2 , $U_{11}^{\text{Te}} = U_{22}^{\text{Te}} = 0.022$ \AA^2 , and $U_{33}^{\text{Te}} = 0.014$ \AA^2 at 300 K) [30]; it is expected that the phonon modes dominated by Tl atoms will be significantly broadened. Indeed, inelastic neutron scattering measurements showed substantial loss of Tl spectral weight on heating (see SM Fig. S7). [30] However, In and Te phonon

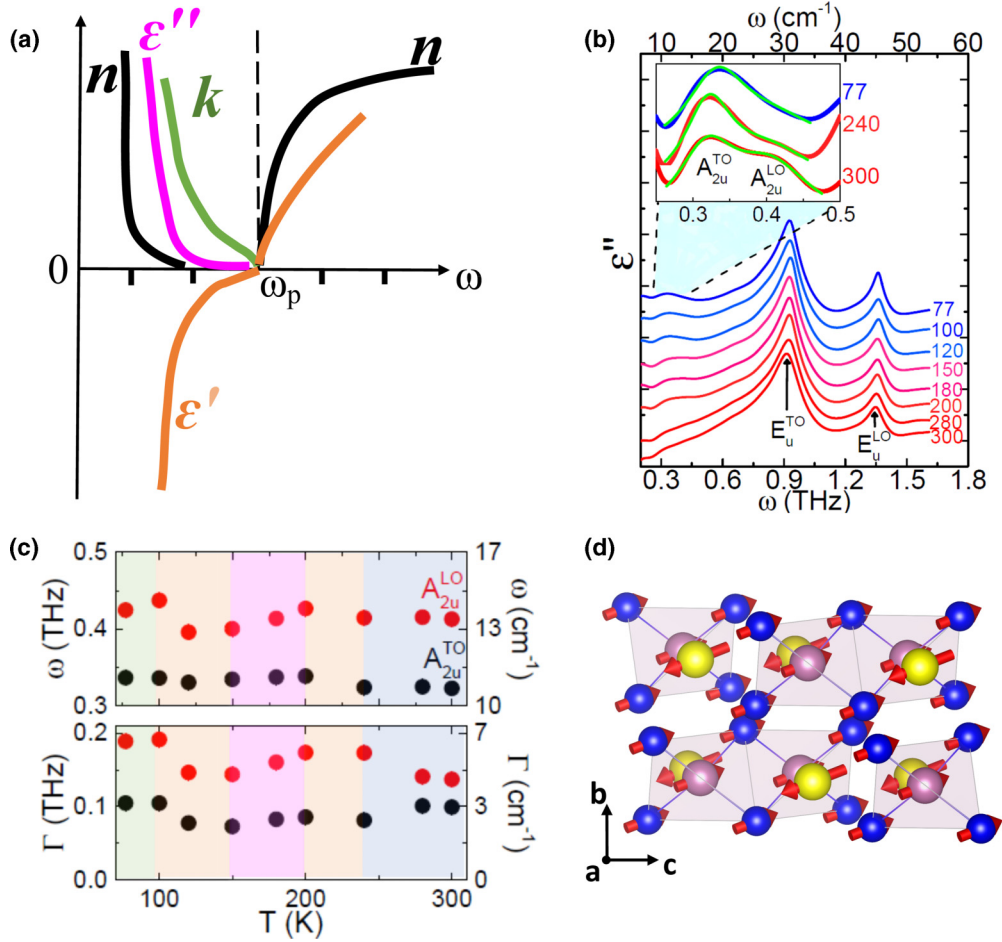


FIG. 3. (a) Qualitative variation of refractive Index $RI = n + ik$ and dielectric constant $\varepsilon = \varepsilon' + i\varepsilon''$ with ω for metals. Here, ω_p is the plasma frequency. (b) ε'' on cooling in low frequency region (0.27-1.8 THz) showing peaks from A_{2u}^{TO} , A_{2u}^{LO} , E_u^{TO} , and E_u^{LO} phonon modes. Inset: Enlarged view in the 0.27–0.5 THz region highlighting A_{2u}^{TO} and A_{2u}^{LO} modes. (c) T dependence of ω (top) and Γ (bottom) for A_{2u}^{TO} (black) and A_{2u}^{LO} (red) modes. Wherever visible, error bars show one standard deviation. (d) Eigenvector of A_{2u}^{TO} and A_{2u}^{LO} modes in the $b-c$ plane showing atomic vibration nearly along the c axis. Note the movement of InTe_4 tetrahedron chains along the $+c$ and $-c$ axis.

peaks, although broadened, did not lose spectral weight. These large anharmonic displacements have been recently probed for superionic conductors (SICs) $(\text{Cu,Ag})\text{CrSe}_2$, where the spectral weight of a mobile ion diminishes, but the underlying sublattice framework remains intact. [66,67] We confirm the rigidity of underlying InTe_4 sublattice by directly probing low-energy (0.3–0.5 THz) A_{2u} symmetry mode that has nearly equal contributions from both Tl and InTe_4 sublattices [see Fig. 3(d)]. Figure 3(b) inset shows an enlarged view of LO-TO splitting of the A_{2u} mode. While a clear loss of spectral weight due to large displacements of the Tl sublattice is visible in Fig. 3(b), the fitted phonon energy (ω) and linewidth (Γ) remain nearly constant in the entire T range (see panel c). If the entire lattice had large anharmonicity, we would have seen a sharp decrease in ω and an increase in Γ on heating. Our measurements and simulations thus confirm anharmonic Tl sublattice vibrations within the rigid framework of InTe_4 tetrahedrons, in line with previous measurements on SICs $(\text{Cu,Ag})\text{CrSe}_2$, where large anharmonicity of mobile Cu/Ag ion sublattice (similar to Tl sublattice here) led to ultralow κ . [66,67]

VI. FINGERPRINTS OF IC MODULATION IN LATTICE RESPONSE

After establishing the multiple phase transitions and T dependence of κ , we now focus on the origin of IC modulation. As evident from our simulated abnormally large dielectric constants (12.16,12.16,13.43), the $+1$ valence state of Tl leaves behind stereochemically active $6s^2$ lone pair. Orbital- and atom-resolved electronic band structure also reveals that Tl s^2 lone pair forms an isolated band and lies below the sp^3 hybridized In and Te states (see SM Fig. S12). Moreover, the Born effective charges of Tl atoms (2.71,2.71,2.11) are nearly two to three times the conventional ionic charges, thus indicating large polarizability of electronic cloud. In (2.47,2.47,4.14) and Te (-2.59,-2.59,-3.12) also have large Born effective charges. The lone pair effects and large polarizability is shown to induce lattice instabilities in rocksalt based ABX_2 compounds (for example, AgInTe_2 and AgSbTe_2) [68] and rocksaltlike IV-VI compound SnSe , [69] and are likely to induce IC modulation in TlInTe_2 . We confirm the IC modulation by directly probing the phonon linewidths (Γ) of A_{2u}^2 , E_u^2 , B_{2g} , and E_g symmetry modes. The A_{2u}^2 and E_u^2 modes involve

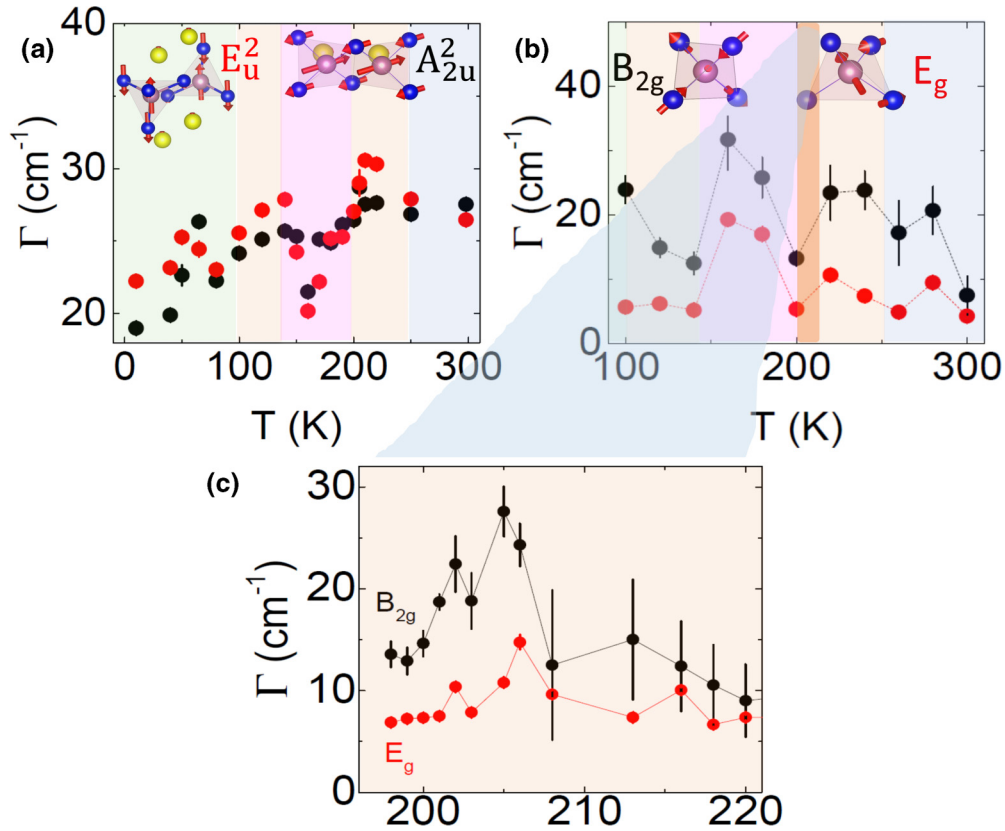


FIG. 4. (a) T dependence of Γ of A_{2u}^2 (black) and E_u^2 (red) modes on cooling showing a dip above T_{IC2} (light pink shaded area). Inset shows their respective atomic vibrations. (b) T dependence of Γ of B_{2g} (black) and E_g (red) modes on cooling showing an increase in Γ above T_{IC2} . (c) Enlarged view of Γ of B_{2g} and E_g modes shown in panel (b) from 200–220 K showing a peak just above T_{II} for both modes. Wherever visible, error bars show one standard deviation.

displacement of Te atoms towards the Tl atoms along the c axis and in the $a-b$ plane [similar to IC modulation, see Fig. 4(a)], respectively, which enables charge sharing between the two and lead to a decrease in the dielectric constant and polarizability. Consequently, both A_{2u}^2 and E_u^2 modes, favoring IC modulation, show a 10 to 30% drop in Γ between T_{II} and T_{IC2} on cooling [Fig. 4(a)]. On the other hand, B_{2g} and E_g modes weaken the sp^3 hybridization between the In and Te atoms, and In-Te bonds become less well-defined. Hence, as shown in Fig. 4(b), the B_{2g} and E_g modes show increase in Γ . We further zoomed in on T range near T_{II} and the same behavior is reproduced [see Fig. 4(c) and SM Fig. S13].

In summary, using comprehensive thermal transport and spectroscopy measurements combined with multichannel thermal transport simulations, we showed sublinear T dependence of κ ($0.7 \leq \alpha \leq 0.8$) above T_D cannot be accounted for by renormalized κ_P and κ_C . The difference is attributed to heat-carrying phason and amplitudon excitations originating from two different translational symmetry in the IC phase of TlInTe₂ that reaches hitherto unreported an unprecedentedly large value of 10-30% of total κ at T_{IC2} . The IC instability is proposed to be triggered by Tl 6s² lone pair and large polarizability, whose signatures are visible in Γ near the phase transition. Our study provides a systematic roadmap to investigate the κ_{IC} (i.e., phason and amplitudon contribution) in insulating, narrow band-gap semiconductors, and metallic IC

phases, in particular for CDW phases where IC modulation is ubiquitous [70–73].

ACKNOWLEDGMENTS

We acknowledge support from Nirma Kumari and Prof. Titas Dasgupta for pellet preparation using hot-press and Deepak and Prof. Sushil Mishra for SEM measurements. N.B. and D.B. thank the financial support from BRNS – DAE under Project No.: 58/14/30/2019-BRNS/11117, and MoE-STARs under Project No.: MoE/STARs-1/345. A.P.R. acknowledges the financial support from IRCC-IITB. S.S.P. acknowledges support of the Department of Atomic Energy, Government of India, under Project Identification No. RTI 4003. K.B. acknowledges support of the Swarnajayanti Fellowship Grant, Science and Engineering Research Board (Grant No. SB/SJF/2019-20/06). H.P.V. and A.J. acknowledge the financial support from National Supercomputing Mission, Government of India (Grant No. DST/NSM/R&D-HPC-Applications/2021/10). The simulations were performed at the SPACETIME-II supercomputing facility at IIT Bombay and PARAM Sanganak supercomputing facility at IIT Kanpur. Raman spectroscopy and XRD experiments were performed at Raman laboratory at IIT Bombay and Indus-2 Synchrotron Radiation Source at RRCAT, Indore, respectively.

- [1] T. Tritt, *Thermal Conductivity: Theory, Properties, and Applications* (Kluwer Academic/Plenum Publishers, New York, 2004).
- [2] P. Klemens, *Solid State Physics: Advances in Research and Applications – Thermal Conductivity and Lattice Vibrational Modes* (Vol. 7, Academic Press Inc., New York, 1958).
- [3] G. Slack, in *CRC Handbook of Thermoelectrics* (CRC Press, 1995).
- [4] S. Mukhopadhyay, D. S. Parker, B. C. Sales, A. A. Puretzy, M. A. McGuire, and L. Lindsay, *Science* **360**, 1455 (2018).
- [5] Y. Wang, R. Lin, P. Zhu, Q. Zheng, Q. Wang, D. Li, and J. Zhu, *Nano Lett.* **18**, 2772 (2018).
- [6] M. Simoncelli, N. Marzari, and F. Mauri, *Nat. Phys.* **15**, 809 (2019).
- [7] T. Lanigan-Atkins, S. Yang, J. Niedziela, D. Bansal, A. May, A. Puretzy, J. Lin, D. Pajeroski, T. Hong, S. Chi, G. Ehlers, and O. Delaire, *Nat. Commun.* **11**, 4430 (2020).
- [8] A. El-Sharkawy, A. Abou El-Azm, M. Kenawy, A. Hillal, and H. Abu-Basha, *Int. J. Thermophys.* **4**, 261 (1983).
- [9] A. H. Romero, E. K. U. Gross, M. J. Verstraete, and O. Hellman, *Phys. Rev. B* **91**, 214310 (2015).
- [10] A. Bruce and R. Cowley, *J. Phys. C* **11**, 3609 (1978).
- [11] P. Toledano and J.-c. Toledano, *Landau Theory Of Phase Transitions, The: Application To Structural, Incommensurate, Magnetic And Liquid Crystal Systems*, Vol. 3 (World Scientific Publishing Company, 1987).
- [12] M. E. Manley, P. J. Stonaha, D. L. Abernathy, S. Chi, R. Sahul, R. P. Hermann, and J. D. Budai, *Nat. Commun.* **9**, 1823 (2018).
- [13] See Supplemental Material at <http://link.aps.org/supplemental/10.1103/PhysRevB.106.214101> for experimental and simulation details and Fig. S1 to S14, which also includes Refs. [14–30].
- [14] M. K. Jana, K. Pal, A. Warankar, P. Mandal, U. V. Waghmare, and K. Biswas, *J. Am. Chem. Soc.* **139**, 4350 (2017).
- [15] J. Rodríguez-Carvajal, *Phys. B: Condens. Matter* **192**, 55 (1993).
- [16] T. Roisnel and J. Rodríguez-Carvajal, in *Materials Science Forum*, Vol. 378 (Transtec Publications; 1999, 2001), pp. 118–123.
- [17] J. Banys, F. Wondre, and G. Guseinov, *Mater. Lett.* **9**, 269 (1990).
- [18] D. Bansal, J. L. Niedziela, X. He, T. Lanigan-Atkins, A. Said, A. Alatas, D. L. Abernathy, Y. Ren, B. Gao, S.-W. Cheong *et al.*, *Phys. Rev. B* **100**, 214304 (2019).
- [19] J. Neu and C. A. Schmuttenmaer, *J. Appl. Phys.* **124**, 231101 (2018).
- [20] M. Fox, *Am. J. Phys.* **70**, 1269 (2002).
- [21] V. I. Korepanov and D. M. Sedlovets, *Analyst* **143**, 2674 (2018).
- [22] A. Jain, *Phys. Rev. B* **102**, 201201 (2020).
- [23] A. J. McGaughey, A. Jain, H.-Y. Kim, and B. Fu, *J. Appl. Phys.* **125**, 011101 (2019).
- [24] P. Giannozzi, O. Andreussi, T. Brumme, O. Bunau, M. B. Nardelli, M. Calandra, R. Car, C. Cavazzoni, D. Ceresoli, M. Cococcioni, N. Colonna, I. Carnimeo, A. D. Corso, S. de Gironcoli, P. Delugas, R. A. D. Jr, A. Ferretti, A. Floris, G. Fratesi, G. Fugallo *et al.*, *J. Phys.: Condens. Matter* **29**, 465901 (2017).
- [25] P. Giannozzi, S. Baroni, N. Bonini, M. Calandra, R. Car, C. Cavazzoni, D. Ceresoli, G. L. Chiarotti, M. Cococcioni, I. Dabo, A. Dal Corso, S. de Gironcoli, S. Fabris, G. Fratesi, R. Gebauer, U. Gerstmann, C. Gougoussis, A. Kokalj, M. Lazzeri, L. Martin-Samos *et al.*, *J. Phys.: Condens. Matter* **21**, 395502 (2009).
- [26] N. K. Ravichandran and D. Broido, *Phys. Rev. B* **98**, 085205 (2018).
- [27] P. Scherpelz, M. Govoni, I. Hamada, and G. Galli, *J. Chem. Theory Comput.* **12**, 3523 (2016).
- [28] K. Pal, Y. Xia, and C. Wolverton, *npj Comput. Mater.* **7**, 1 (2021).
- [29] H. Matsumoto, K. Kurosaki, H. Muta, and S. Yamanaka, *J. Appl. Phys.* **104**, 073705 (2008).
- [30] M. Dutta, M. Samanta, T. Ghosh, D. J. Voneshen, and K. Biswas, *Angew. Chem.* **133**, 4305 (2021).
- [31] C. D. Amarasekara and P. H. Keesom, *Phys. Rev. B* **26**, 2720 (1982).
- [32] M. Apostol, *Commun. Theor. Phys.* **20**, 249 (1993).
- [33] B. Hennion, J. P. Pouget, and M. Sato, *Phys. Rev. Lett.* **68**, 2374 (1992).
- [34] A. Smontara, K. Biljaković, and S. N. Artemenko, *Phys. Rev. B* **48**, 4329 (1993).
- [35] X. Xu, A. F. Bangura, C. Q. Niu, M. Greenblatt, S. Yue, C. Panagopoulos, and N. E. Hussey, *Phys. Rev. B* **85**, 195101 (2012).
- [36] G. Grimvall, *The Electron-Phonon Interaction in Metals* (North-Holland, Amsterdam, 1981).
- [37] F. Giustino, *Rev. Mod. Phys.* **89**, 015003 (2017).
- [38] P. Bak, *Rep. Prog. Phys.* **45**, 587 (1982).
- [39] V. Heine and J. McConnell, *J. Phys. C* **17**, 1199 (1984).
- [40] K. Hamano, Y. Ikeda, T. Fujimoto, K. Ema, and S. Hirotsu, *J. Phys. Soc. Jpn.* **49**, 2278 (1980).
- [41] J. R. Hardy, *Ferroelectrics* **117**, 53 (1991).
- [42] V. Katkanant, P. Edwardson, J. Hardy, and L. Boyer, *Phase Trans.* **15**, 103 (1989).
- [43] J. Scott, *Rep. Prog. Phys.* **42**, 1055 (1979).
- [44] H. J. Schulz, *Phys. Rev. B* **22**, 5274 (1980).
- [45] J. Axe, *Philos. Trans. R. Soc. Lond. B* **290**, 593 (1980).
- [46] M. Quilichini and R. Currat, *Solid State Commun.* **48**, 1011 (1983).
- [47] I. Gregora, J. Hlinka, and B. Březina, *Ferroelectrics* **302**, 155 (2004).
- [48] M. Baggioli and M. Landry, *SciPost Physics* **9**, 062 (2020).
- [49] T. Janssen, *Zeitschrift für Kristallographie* **223**, 742 (2008).
- [50] A. Panich, *J. Phys.: Condens. Matter* **20**, 293202 (2008).
- [51] M. Wu, Enamullah, and L. Huang, *Phys. Rev. B* **100**, 075207 (2019).
- [52] M. Ishikawa, T. Nakayama, K. Wakita, Y. Shim, and N. Mamedov, *J. Appl. Phys.* **123**, 161575 (2018).
- [53] K. Mamedov, A. Abdullaev, and E. Kekimova, *Phys. Status Solidi (a)* **94**, 115 (1986).
- [54] V. Aliev, M. Aldzhanov, and S. Aliev, *Pis'ma Zh. Eksp. Teor. Fiz.* **45**, 418 (1987).
- [55] N. Mamedov and A. Panich, *Phys. Status Solidi (a)* **117**, K15 (1990).
- [56] O. Z. O. Alekperov, M. A. O. Aljanov, and E. M. A. G. Kerimova, *Turk. J. Phys.* **22**, 1053 (1998).
- [57] M. Aldzhanov, K. Mamedov, and A. Abdurragimov, *Phys. Stat. Sol. (b)* **131**, K35 (1985).
- [58] G. Guseinov, E. Mooser, E. Kerimova, R. Gamidov, I. Alekseev, and M. Ismailov, *Phys. Stat. Sol. (b)* **34**, 33 (1969).
- [59] F. Abdullaev, T. Kerimova, and N. Abdullaev, *Phys. Solid State* **47**, 1221 (2005).

- [60] G. Ding, J. He, Z. Cheng, X. Wang, and S. Li, *J. Mater. Chem. C* **6**, 13269 (2018).
- [61] E. Godzhaev, G. K. Binnatli, M. Guseinov, and R. Kerimova, *Journal of Engineering Physics and Thermophysics* **76**, 441 (2003).
- [62] Y. Imry and M. Wortis, *Phys. Rev. B* **19**, 3580 (1979).
- [63] A. Al-Ghamdi, F. Al-Hazmi, S. Al-Heniti, A. Nagat, F. Bahabri, M. Mobarak, and S. Alharbi, *JKAU: Science* **20**, 27 (2008).
- [64] J. Zhou, H. D. Shin, K. Chen, B. Song, R. A. Duncan, Q. Xu, A. A. Maznev, K. A. Nelson, and G. Chen, *Nat. Commun.* **11**, 1 (2020).
- [65] M. Dresselhaus, <http://web.mit.edu/afs/athena/course/6/6.732/www/opt.pdf>.
- [66] J. Niedziela, D. Bansal, A. May, J. Ding, T.L.-Atkins, G. Ehlers, D. Abernathy, A. Said, and O. Delaire, *Nat. Phys.* **15**, 73 (2019).
- [67] J. Ding, J. L. Niedziela, D. Bansal, J. Wang, X. He, A. F. May, G. Ehlers, D. L. Abernathy, A. Said, A. Alatas *et al.*, *Proc. Natl. Acad. Sci.* **117**, 3930 (2020).
- [68] M. Nielsen, V. Ozolins, and J. Heremans, *Energy & Environmental Science* **6**, 570 (2013).
- [69] C. Li, J. Hong, A. May, D. Bansal, J. Ma, T. Hong, S. Chi, G. Ehlers, and O. Delaire, *Nat. Phys.* **11**, 1063 (2015).
- [70] N. Ru, C. L. Condrón, G. Y. Margulis, K. Y. Shin, J. Laverock, S. B. Dugdale, M. F. Toney, and I. R. Fisher, *Phys. Rev. B* **77**, 035114 (2008).
- [71] C.-W. Chen, J. Choe, and E. Morosan, *Rep. Prog. Phys.* **79**, 084505 (2016).
- [72] A. P. Roy, N. Bajaj, R. Mittal, P. D. Babu, and D. Bansal, *Phys. Rev. Lett.* **126**, 096401 (2021).
- [73] G. Lander, E. Fisher, and S. Bader, *Adv. Phys.* **43**, 1 (1994).